

**Effect of the Landau quantization of electrons on the inner crusts of hot neutron stars**Rana Nandi <sup>1,\*</sup>, Somnath Mukhopadhyay <sup>2,†</sup> and Sarmistha Banik <sup>3,‡</sup><sup>1</sup>*Polba Mahavidyalaya, Hooghly, West Bengal 712148, India*<sup>2</sup>*NIT Tiruchirappalli, Tamil Nadu 620015, India*<sup>3</sup>*Department of Physics, BITS Pilani, Hyderabad Campus, Hyderabad-500078, India*

(Received 3 November 2020; revised 18 June 2021; accepted 21 July 2021; published 12 August 2021)

In the present work we study the effects of strongly quantizing magnetic fields and finite temperature on the properties of inner crusts of hot neutron stars. In particular, we study the effects of Landau quantization of electrons on the composition of the NS inner crusts. The inner crust of a neutron star contains neutron-rich nuclei arranged in a lattice and embedded in gases of free neutrons and electrons. We describe the system within the Wigner-Seitz (WS) cell approximation. The nuclear energy is calculated using Skyrme model with SkM\* interaction. To isolate the properties of nuclei we follow the subtraction procedure presented by Bonche, Levit, and Vautherin [*Nuc. Phys. A* **427**, 278 (1984); **436**, 265 (1985)], within the Thomas-Fermi approximation. We obtain the equilibrium properties of the inner crust for various density, temperatures, and magnetic fields by minimizing the free energy of the WS cell satisfying the charge neutrality and  $\beta$ -equilibrium conditions. We infer that at a fixed baryon density and temperature, a strong quantizing magnetic field reduces the cell radii, neutron, and proton numbers in the cell compared with the field free case. However, the nucleon number in the nucleus increases in the presence of a magnetic field. The free energy per nucleon also decreases in the magnetized inner crust. On the other hand, we find that finite temperature tends to smear out the effects of magnetic field. Our results can be important in the context of  $r$ -process nucleosynthesis in the binary neutron star mergers.

DOI: [10.1103/PhysRevC.104.025803](https://doi.org/10.1103/PhysRevC.104.025803)**I. INTRODUCTION**

Pulsars are highly magnetized rapidly rotating neutron stars having surface magnetic fields  $\approx 10^{12}$  G. There is a class of neutron stars named magnetars consisting of anomalous x-ray pulsars (AXPs) and soft gamma-ray repeaters (SGRs) with even higher surface magnetic field  $\approx 10^{14}$ – $10^{15}$  G [1,2]. Such intense magnetic fields can be generated by a dynamo mechanism in hot and newly born neutrons stars (NS) after core-collapse supernova [1,3,4]. The maximum magnetic field that can exist inside the core is set by the virial theorem [5,6] and for a typical NS of mass  $1.5M_{\odot}$  and radius 10 km the limiting field could be as high as  $\approx 10^{18}$  G.

The properties of matter in such a high magnetic field is an interesting field of research in theoretical astrophysics. The magnetic field is termed quantizing in the sense that the charged particles move in quantized orbits known as Landau levels in the direction perpendicular to the magnetic field [7–10]. The charged particles become relativistic and Landau quantized when the cyclotron energy becomes comparable to the rest mass energy of the particle. Landau quantization changes the phase space and density of states and hence modifies the thermodynamic and transport properties of highly magnetized matter. Effects of Landau quantization

have been studied extensively on the outer crust using the magnetized Baym-Pethick-Sutherland (BPS) equation of state (EoS) [6] and also using atomic mass models of Hartree-Fock-Bogoliubov [11]. In the NS core Landau quantization has been studied using the relativistic mean field model [12–14]. The effects of strong magnetic fields and proton fraction on the inner crust of magnetized neutron stars have been studied extensively [15–17].

In this study we focus on the inner crust of a hot neutron star in the presence of a quantizing magnetic field and at finite temperature. The inner crust is composed of nuclei immersed in a neutron and electron gas. The matter is  $\beta$ -equilibrated and charge neutral and the nuclei are also in mechanical equilibrium with the neutron gas. In order to calculate the equilibrium properties of nuclei in the thermodynamic method, we follow the subtraction procedure of Bonche, Levit, and Vautherin (BLV) [18–20]. In this method, the nuclear properties are isolated from the nucleus plus gas phase using the subtraction procedure in a temperature-dependent Hartree-Fock theory [18,19] as well as in zero and finite temperature extended Thomas-Fermi (TF) calculations [20]. The subtraction procedure was extended to isolated nuclei embedded in a neutron gas [21] and to nuclei in the inner crust at zero temperature [22]. In a later work the subtraction procedure is also applied to nuclei in a strongly magnetized inner crust taking into effect the Landau quantization of degenerate electrons at zero temperature [23]. Here, we extend the subtraction procedure to include strongly quantizing magnetic field and finite temperature effects using the finite-temperature magnetized TF

\*nandi.rana@gmail.com

†somnath@nitt.edu

‡sarmistha.banik@hyderabad.bits-pilani.ac.in

formalism. This is relevant for inner crusts of newly formed hot magnetars and binary neutron star mergers where the crustal matter can be heated and the magnetic field can get amplified during the merging process [24].

## II. FORMALISM

We study the composition of the inner crust of NS for different temperatures and magnetic fields. The inner crust consists of nuclei arranged in a lattice and immersed in free gases of electrons and neutrons. For finite temperatures there might be free protons as well. We employ the Wigner-Seitz (WS) cell approximation where the lattice is divided into spherical cells. Each WS cell is considered to be charge neutral containing a nucleus at its center and the interaction between cells is ignored. We assume that the matter is in  $\beta$  equilibrium. We further assume that the whole system is placed in a uniform magnetic field. A strong magnetic field affects electrons as their motion in the plane perpendicular to the field get quantized into Landau levels. However, protons are affected only through the charge neutrality condition.

Due to the presence of nucleonic gases in the inner crust, the spherical cell itself does not define a nucleus. How to isolate the properties of nuclei in such a scenario was shown within both the Hartree-Fock (HF) prescription [18,19] and TF formalism [20]. This is based on the fact that at a given temperature and chemical potential there exists two solutions to the HF or TF equations, one solution corresponds to the nucleus in equilibrium with the nucleon gases while the other represents the nucleon gases alone. The nucleus solution is obtained from the difference of two solutions. More specifically, the nuclear properties like charge number ( $Z$ ), mass numbers ( $A$ ), rms radii, etc., are calculated from the subtracted density  $\rho_{\text{NG}}(r) - \rho_{\text{G}}(r)$ , where  $\rho_{\text{NG}}(r)$  and  $\rho_{\text{G}}(r)$  are density profiles in the nucleus+gas phase and gas only phase, respectively, and are obtained by minimizing the corresponding thermodynamic potentials  $\Omega_{\text{NG}}(\rho_{\text{NG}})$  and  $\Omega_{\text{G}}(\rho_{\text{G}})$  as detailed below. We refer to this as the BLV separation procedure.

The thermodynamic potential can be written as

$$\Omega = \mathcal{F} - \sum_q \mu_q A_q, \quad (1)$$

where  $\mathcal{F}$  is the free energy,  $q = (n, p)$  stands for neutrons and protons, and  $\mu_q$  are  $A_q$  are the corresponding chemical potentials and numbers, respectively. The total free energy of the cell is a function of average baryon number density ( $\langle \rho \rangle$ ), temperature ( $T$ ), and proton fraction ( $Y_p$ ) and can be expressed as

$$\mathcal{F}(\langle \rho \rangle, Y_p, T) = \int [\mathcal{H}(r) - Ts(r) + \mathcal{E}_c(r) + f_e(\rho_e)] d\mathbf{r}. \quad (2)$$

Here,  $\mathcal{H}$  refers to the nuclear energy density excluding the Coulomb energy,  $s$  is the entropy density of the nucleons,  $\mathcal{E}_c$  the Coulomb energy density of the system,  $f_e = \varepsilon_e - Ts_e$  is the free energy density of the electrons, and  $\rho_e$  is the electron number density. Here,  $\varepsilon_e$  is the energy density and  $s_e$  entropy density of the electrons.

For the nuclear energy density  $\mathcal{H}$ , we adopt the Skyrme energy density functional which is written as [25,26]

$$\begin{aligned} \mathcal{H}(r) = & \sum_q \frac{\hbar^2}{2m_q^*} \tau_q + \frac{1}{2} t_0 \left[ \left(1 + \frac{x_0}{2}\right) \rho^2 - \left(x_0 + \frac{1}{2}\right) \sum_q \rho_q^2 \right] \\ & - \frac{1}{16} \left[ t_2 \left(1 + \frac{x_2}{2}\right) - 3t_1 \left(1 + \frac{x_1}{2}\right) \right] (\nabla \rho)^2 \\ & - \frac{1}{16} \left[ 3t_1 \left(x_1 + \frac{1}{2}\right) + t_2 \left(x_2 + \frac{1}{2}\right) \right] \sum_q (\nabla \rho_q)^2 \\ & + \frac{1}{12} t_3 \rho^\alpha \left[ \left(1 + \frac{x_3}{2}\right) \rho^2 - \left(x_3 + \frac{1}{2}\right) \sum_q \rho_q^2 \right]. \quad (3) \end{aligned}$$

We employ the SkM\* interaction, for which the parameters  $x_0, x_1, x_2, x_3, t_0, t_1, t_2, t_3$ , and  $\alpha$  can be found in [25]. Properties of SkM\* at saturation density ( $0.16 \text{ fm}^{-3}$ ) are: binding energy per nucleon  $B/A = -15.8 \text{ MeV}$ , symmetry binding energy per nucleon  $B/A = -15.8 \text{ MeV}$ , symmetry energy  $J = 30 \text{ MeV}$ , isoscalar incompressibility  $K = 216 \text{ MeV}$ , effective mass ratio  $m^*/m = 0.79$ , and symmetry energy slope  $L = 46 \text{ MeV}$ . In Eq. (3),  $\rho = \rho_p + \rho_n$  and  $m_q^*$  is the effective mass defined as

$$\begin{aligned} \frac{m}{m_q^*(r)} = & 1 + \frac{m}{2\hbar^2} \left\{ \left[ t_1 \left(1 + \frac{x_1}{2}\right) + t_2 \left(1 + \frac{x_2}{2}\right) \right] \rho \right. \\ & \left. + \left[ t_2 \left(x_2 + \frac{1}{2}\right) - t_1 \left(x_1 + \frac{1}{2}\right) \right] \rho_q \right\}. \quad (4) \end{aligned}$$

The kinetic energy density  $\tau_q$  takes the form in TF approximation as

$$\begin{aligned} \tau_q = & \frac{3}{5} (3\pi^2)^{2/3} \rho_q^{5/3} \quad \text{for } T = 0, \\ = & \frac{1}{2\pi^2} \left( \frac{2m_q^* T}{\hbar^2} \right)^{5/2} J_{3/2}(\eta_q) \quad \text{for } T \neq 0, \quad (5) \end{aligned}$$

where  $\eta_q$  is the fugacity that is obtained from the chemical potential and single particle potential of nucleons  $V_q$  as

$$\eta_q(r) = (\mu_q - V_q(r))/T. \quad (6)$$

The number density of nucleons is given by

$$\rho_q(r) = \frac{1}{2\pi^2} \left( \frac{2m_q^* T}{\hbar^2} \right)^{3/2} J_{1/2}(\eta_q). \quad (7)$$

The functions  $J_k(\eta_q)$  appearing in Eqs. (5) and (7) are Fermi integrals:

$$J_k(\eta_q) = \int_0^\infty \frac{x^k}{\exp(x - \eta_q) + 1} dx. \quad (8)$$

The entropy density of the nucleons is related to fugacity and number density as

$$s(r) = \sum_q [(5/3)J_{3/2}(\eta_q)/J_{1/2}(\eta_q) - \eta_q] \rho_q. \quad (9)$$

The third term in the integrand of Eq. (2) is the Coulomb energy density of the charged particles and is given by

$$\mathcal{E}_c(r) = \frac{1}{2} (\rho_p(r) - \rho_e) \int (\rho_p(r') - \rho_e) \frac{e^2}{|\mathbf{r} - \mathbf{r}'|} d\mathbf{r}'. \quad (10)$$

We neglect the exchange term for the Coulomb energy density.

The density profiles of nucleus+gas (NG) phase  $\rho_{\text{NG}}^q$  and gas (G) phase  $\rho_{\text{G}}^q$  are obtained from the variational equations

$$\frac{\delta\Omega_{\text{NG}}}{\delta\rho_{\text{NG}}^q} = 0, \quad (11)$$

$$\frac{\delta\Omega_{\text{G}}}{\delta\rho_{\text{G}}^q} = 0, \quad (12)$$

where  $\Omega_{\text{NG}}$  and  $\Omega_{\text{G}}$  are the thermodynamic potentials of the corresponding phases. This results in the following coupled equations [22,23]:

$$T\eta_{\text{NG}}^q(r) + V_{\text{NG}}^q + V_{\text{NG}}^c(\rho_{\text{NG}}^p, \rho_e) = \mu_q, \quad (13)$$

$$T\eta_{\text{G}}^q(r) + V_{\text{G}}^q + V_{\text{G}}^c(\rho_{\text{NG}}^p, \rho_e) = \mu_q. \quad (14)$$

At  $T = 0$  these two equations simplify to

$$(3\pi^2)^{2/3} \frac{\hbar^2}{2m_q^*} (\rho_{\text{NG}}^q)^{2/3} + V_{\text{NG}}^q + V_{\text{NG}}^c(\rho_{\text{NG}}^p, \rho_e) = \mu_q, \quad (15)$$

$$(3\pi^2)^{2/3} \frac{\hbar^2}{2m_q^*} (\rho_{\text{NG}}^q)^{2/3} + V_{\text{G}}^q + V_{\text{G}}^c(\rho_{\text{NG}}^p, \rho_e) = \mu_q, \quad (16)$$

where  $V_{\text{NG}}^q$  and  $V_{\text{G}}^q$  are the nuclear part of the single particle potentials in the nucleus+gas and gas phases, respectively, and  $V_{\text{NG}}^c$  and  $V_{\text{G}}^c$  correspond to the Coulomb part of the single particle potential for two phases and are given by the same expression as [22,23]

$$V^c(r) = \int [\rho_{\text{NG}}^p(r') - \rho_e] \frac{e^2}{|\mathbf{r} - \mathbf{r}'|} d\mathbf{r}'. \quad (17)$$

The average chemical potential for the  $q$ th nucleon is given by

$$\mu_q = \frac{1}{A_q} \int [T\eta_{\text{NG}}^q(r) + V_{\text{NG}}^q(r) + V_{\text{NG}}^c(r)] \rho_{\text{NG}}^q(r) d\mathbf{r}, \quad (18)$$

where  $A_q$  refers to  $N_{\text{cell}}$  or  $Z_{\text{cell}}$ , where  $N_{\text{cell}}$  and  $Z_{\text{cell}}$  are neutron and proton numbers in the WS cell, respectively, which can easily be obtained from the average baryon density  $\langle\rho\rangle$ , proton fraction  $Y_p$  and the cell radius  $R_c$  as

$$Z_{\text{cell}} = Y_p \langle\rho\rangle V_{\text{cell}},$$

$$N_{\text{cell}} = (1 - Y_p) \langle\rho\rangle V_{\text{cell}}, \quad \text{and} \quad V_{\text{cell}} = \frac{4}{3}\pi R_c^3, \quad (19)$$

where  $V_{\text{cell}}$  is the volume of the cell. The total number of nucleons in the cell is  $A_{\text{cell}} = N_{\text{cell}} + Z_{\text{cell}}$ .

Finally, number of neutrons ( $N$ ) and protons ( $Z$ ) in a nucleus are obtained from the subtracted densities following the BLV prescription as

$$Z = \int [\rho_p^{\text{NG}}(r) - \rho_p^{\text{G}}(r)] d\mathbf{r},$$

$$N = \int [\rho_n^{\text{NG}}(r) - \rho_n^{\text{G}}(r)] d\mathbf{r}, \quad (20)$$

so that the mass number of the nucleus is  $A = N + Z$ .

We assume the matter to be in  $\beta$  equilibrium, the chemical potential  $\mu$  of the species are constrained by the relation

$$\mu_e = \mu_n - \mu_p + \Delta m, \quad (21)$$

where  $\Delta m$  is the mass difference between neutrons and protons.

### A. Effect of quantizing magnetic field

The properties of inner crust are significantly influenced in the presence of strong quantizing magnetic field. We assume a uniform magnetic field  $(0, 0, B)$  in the crust. The motion of electrons is Landau quantized in the plane perpendicular to the magnetic field, which indirectly affects the properties of protons in the charge neutral WS cells and hence the nuclei. For  $B > B_c = m_e^2/e \simeq 4.414 \times 10^{13}$  G (with  $\hbar = c = 1$ ), the transverse motion of the electrons becomes relativistic [6]. The quantized energy levels of the electrons with momentum  $p_z$  for  $\nu$ th Landau level is given by (with  $B_* = B/B_c$ )

$$E_e(\nu, p_z) = [p_z^2 + m_e^2(1 + 2\nu B_*)]^{1/2}. \quad (22)$$

The number density of electrons in the magnetic field at finite temperature can be written as [27]

$$\rho_e = \frac{m_e^2 B_*}{4\pi^2} \sum_{\nu=0}^{\infty} g_{\nu} \int_{-\infty}^{\infty} f dp_z, \quad (23)$$

where

$$f = \frac{1}{1 + e^{\beta(E_e - \mu_e)}} \quad (24)$$

is the Fermi-Dirac distribution function with  $\beta = 1/(k_B T)$ ,  $\mu_e$  is the electron chemical potential,  $g_{\nu}$  is the spin degeneracy of the Landau level ( $g_0 = 1$  and  $g_{\nu} = 2$  for  $\nu \geq 1$ ). At  $T = 0$  the above expression simplifies to

$$\rho_e = \frac{m_e^2 B_*}{2\pi^2} \sum_{\nu=0}^{\nu_{\text{max}}} g_{\nu} p_f(\nu), \quad (25)$$

where  $p_f(\nu)$  is the maximum  $z$  component of electron momentum and is related to the chemical potential as

$$p_f^2(\nu) + m_e^2(1 + 2\nu B_*) = \mu_e^2 \quad (26)$$

and  $\nu_{\text{max}}$  is highest Landau level that can be populated for a given  $B_*$  and  $\mu_e$  and is obtained by noting that  $p_f^2(\nu) \geq 0$ :

$$\nu_{\text{max}} = \frac{\mu_e^2 - m_e^2}{2m_e^2 B_*}. \quad (27)$$

The energy density of electrons is obtained from

$$\varepsilon_e = \frac{m_e^2 B_*}{4\pi^2} \sum_{\nu=0}^{\infty} g_{\nu} \int_{-\infty}^{\infty} f E_e(\nu, p_z) dp_z \quad \text{for } T \neq 0, \quad (28)$$

$$= \frac{m_e^2 B_*}{2\pi^2} \sum_{\nu=0}^{\infty} g_{\nu} \int_0^{p_f(\nu)} E_e(\nu, p_z) dp_z \quad \text{for } T = 0. \quad (29)$$

## III. RESULTS

We present the properties of matter in the inner crusts of neutron stars under the influence of strong magnetic fields and finite temperature. Particularly, we study the effects of

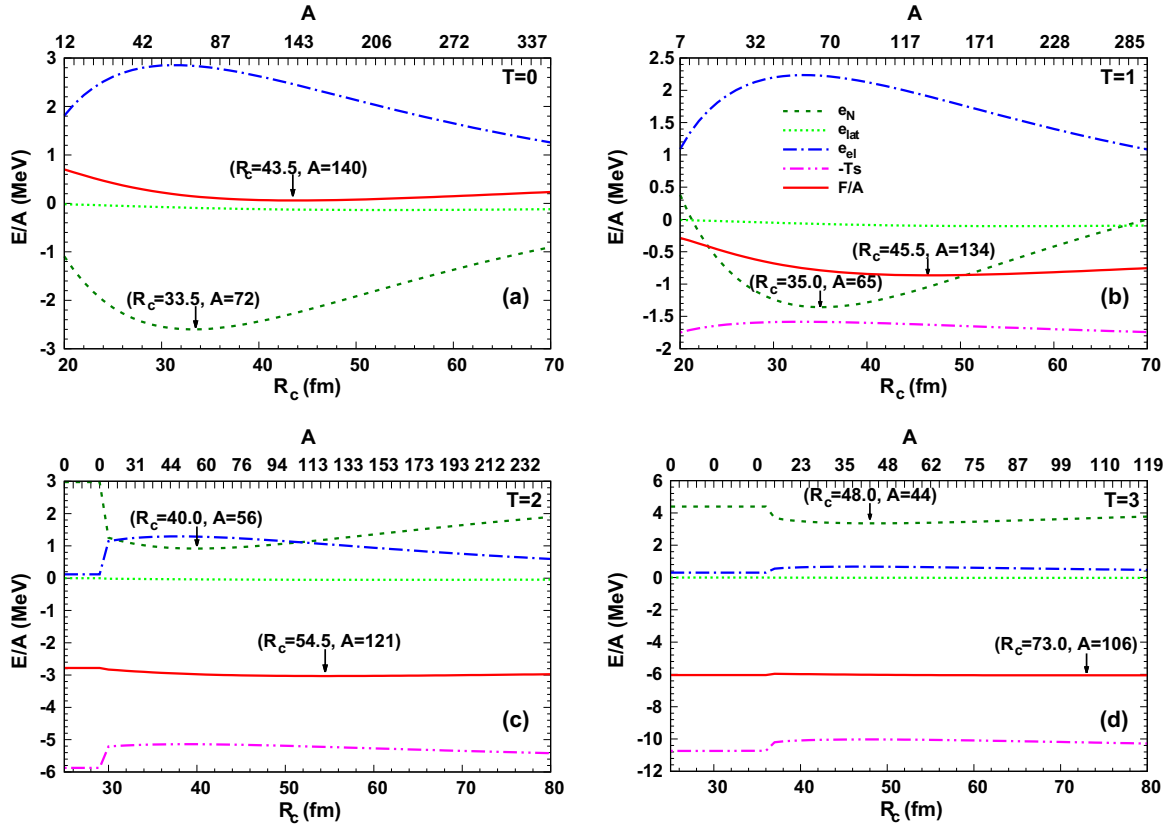


FIG. 1. Different contributions to the free energy per nucleon as a function of  $R_c$  and  $A$  (upper x axis) for  $T = 0$ –3 MeV,  $B = 0$ , and  $\langle \rho \rangle = 0.001 \text{ fm}^{-3}$ .

Landau quantization of electrons on the composition of the inner crusts of NS. We have neglected here the Landau quantization of protons. For this purpose we consider magnetic fields  $B_* = 10, 100, 10^3$ , and  $10^4$ . The effect of magnetic field is noticeable if only first few levels are populated. The highest Landau level  $\nu_m$  populated at a given  $B_*$  can be calculated from Eq. (27) for  $T = 0$ . On the other hand, one needs to evaluate infinite sums over Landau levels to calculate number and energy densities of electrons [Eqs. (23) and (28)], for  $T \neq 0$ . In practice, only finite number of levels contribute when the magnetic field is strong. In the numerical implementation we set the Fermi function [Eq. (24)] to zero when  $\beta(E_e(\nu, p_z) - \mu_e) \geq 30$ . This condition along with Eq. (22) leads to the highest Landau level as

$$\nu_{\max} = \frac{1}{2B_*} \left[ \left( \frac{30T + \mu_e}{m_e} \right)^2 - 1 \right]. \quad (30)$$

Equation (27) is recovered by putting  $T = 0$ .

We demonstrate the results only for  $B_* = 10^4$  when only the zeroth Landau level is populated (at least for  $T = 0$ ). For lower values of  $B_*$  there is no visible effect as several Landau levels are populated by electrons. For comparison, we also show the results for  $B_* = 0$  cases. We consider the crust temperature in the range of 0–5 MeV. In order to obtain the equilibrium configuration for a given average number density ( $\langle \rho \rangle$ ), temperature ( $T$ ), and magnetic field ( $B_*$ ), we minimize the free energy of the WS cell by varying  $Y_p$  and  $R_c$  while

satisfying the conditions of charge neutrality and  $\beta$  equilibrium. The free energy minimum is governed by the contribution of different terms:

$$F/A_{\text{cell}} = e_N + e_{\text{lat}} + e_{\text{el}} - Ts, \quad (31)$$

where  $e_N$  is nuclear energy per nucleon including the Coulomb energy of protons,  $e_{\text{lat}}$  is the lattice energy per nucleon which consists of electron-proton and electron-electron Coulomb energies,  $e_{\text{el}}$  is the kinetic energy of electrons per nucleon, and  $s$  is the entropy per nucleon including the entropy of electrons. In Fig. 1, we show the variation of all the components of free energy per nucleon with the cell radius or equivalently  $A_{\text{cell}}$  (since,  $A_{\text{cell}} = V_{\text{cell}} \langle \rho \rangle$ ) at a density  $\langle \rho \rangle = 0.001 \text{ fm}^{-3}$  and at different temperatures ( $T = 0$ –3 MeV) for the nonmagnetic case. The upper x axis presents the corresponding mass number of nuclei obtained from the subtracted densities [see Eq. (20)]. It is seen from the figure that for each  $T$ ,  $e_N$  has a minimum at a certain  $R_c$ . Since, the nuclear mass number  $A$  (see upper x axis) increases monotonically with  $R_c$ , the minimum in  $e_N$  corresponds to the nucleus for which the nuclear binding energy per nucleon is minimum. These nuclei are very neutron-rich and get smaller with increasing  $T$ . The free energy minima are at larger  $R_c$  as they originate from the competition between different terms, but mostly dominated by  $e_N$  and  $e_{\text{el}}$  and also  $Ts$  at finite temperature. An interesting feature appears at  $T = 2$  MeV, where a sudden change in each component of free energy is observed at  $R_c = 30$  fm. The upper x axis reveals that for  $R_c < 30$  fm  $A = 0$ , which

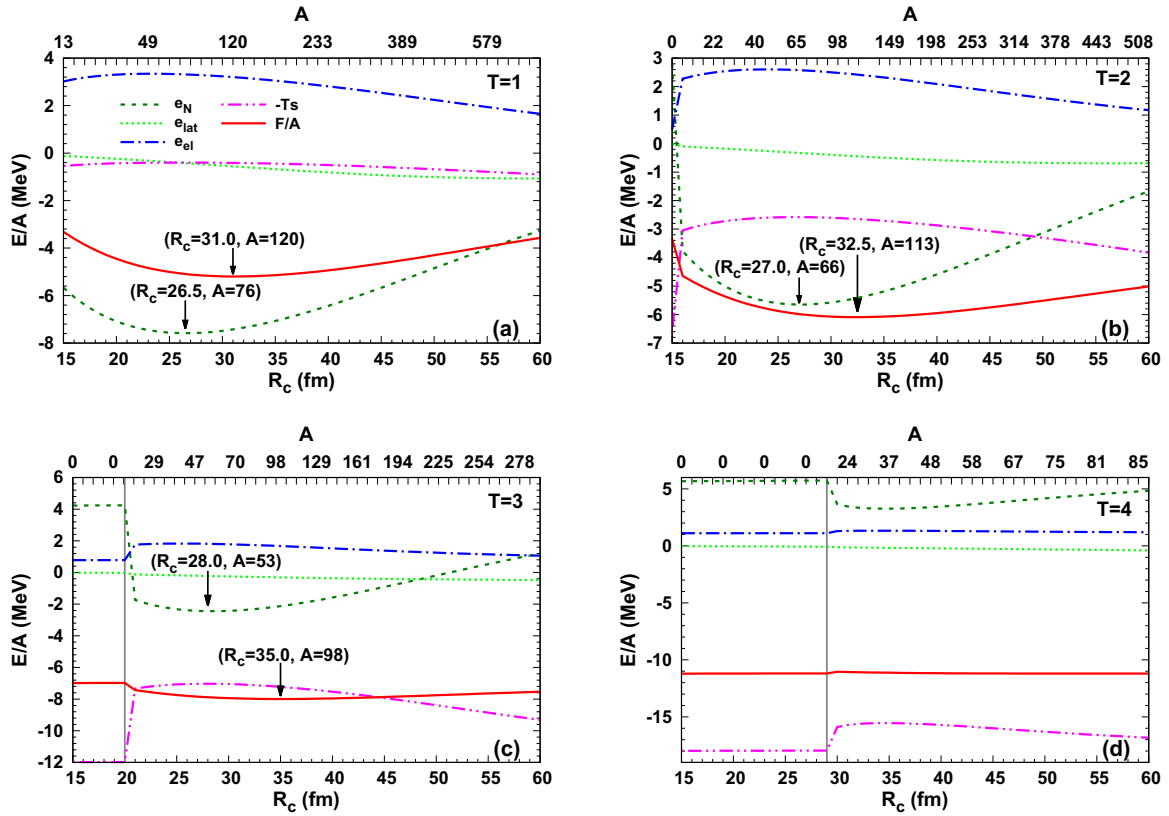


FIG. 2. Same as Fig. 1 but for  $T = 1-4$  MeV, and  $B_* = 10^4$ .

essentially means that no nucleus exists till that  $R_c$  and the matter is completely in the gas state, instead. However, the complete gas state has higher free energy than the nucleus+gas state for which the free energy is minimum at  $R_c = 54.5$  fm. Similar behavior is found at  $T = 3$  MeV, where nuclei come into the picture only after  $R_c = 36$  fm. Still we find that the free energy minimum corresponds to nuclear+gas solution at  $R_c = 73$  fm. The free energy difference between the complete gas state and the nuclear+gas state decreases with  $T$ . At  $T = 2$  MeV the minimum values of free energies in the two states are  $-2.780$  and  $-3.029$  MeV. Whereas, for  $T = 3$  MeV the corresponding values are  $-6.038$  and  $-6.057$  MeV. For  $T = 4$  MeV or higher (not shown here) only the gas solution exists. Therefore, we can say that the transition temperature from the liquid to the gas phase lies between  $T = 3$  and  $4$  MeV at this density. This agrees with the results of other studies [28].

In Fig. 2 we present the variation of free energy and its different components with  $R_c$  as in Fig. 1, but now in the presence of magnetic field with  $B_* = 10^4$ . We do not show the plot for  $T = 0$ , since there are no drip neutrons at  $\langle \rho \rangle = 0.001 \text{ fm}^{-3}$ , unlike the nonmagnetic case. This is consistent with the earlier studies where it was found that strong magnetic fields shift the neutron drip-point to higher densities [29]. Similar to the nonmagnetic case we find that with increasing  $T$  the cell radius corresponding to both the  $e_N$  minimum and the free energy minimum increase, whereas the mass number of the equilibrium nucleus decreases. At  $T = 3$ , matter is uniform till  $R_c = 20$  fm and beyond that nucleus

appears with free energy minimum at  $R_c = 35$  fm, where  $A = 98$ . On the other hand, at  $T = 4$  uniform gas solution extends up to  $29$  fm and has lower free energy than the solution with nucleus. Hence, the equilibrium corresponds to gas solution, i.e., uniform matter at this temperature and density.

Comparison between Figs. 1 and 2 shows that when  $B_* = 10^4$  the minima in  $e_N$  and free energy are obtained at lower  $R_c$ . It can also be seen that  $e_N$  plays more dominant role in deciding the free energy minimum. As a result, the  $R_c$  corresponding to the free energy minima are not very far from that of  $e_N$ , unlike nonmagnetic scenario. Comparing these two figures we also observe that a strong magnetic field affects all the components of free energy. But the effect is found to be most significant on  $e_N$  which gets appreciably reduced when magnetic field of  $B_* = 10^4$  is applied. To understand the reason we note that for a given  $\langle \rho \rangle$  and  $Y_p$  although the electron density is the same for both the scenarios (since  $\rho_e = Y_p \langle \rho \rangle$ ), the electron chemical potential  $\mu_e$  decreases significantly. For instance, in the present example of  $\langle \rho \rangle = 0.001 \text{ fm}^{-3}$ , the  $e_N$  minimum at  $T = 1$  MeV for the nonmagnetic case corresponds to  $R_c = 35$  fm,  $Y_p = 0.102$ ,  $\rho_e = 1.02 \times 10^{-4} \text{ fm}^{-3}$ , and  $\mu_e = 28$  MeV. When the magnetic field of magnitude  $B_* = 10^4$  is switched on keeping the values of  $\langle \rho \rangle$ ,  $T$ ,  $R_c$ , and  $Y_p$  same we find that  $\mu_e$  reduces from  $28$  to  $6$  MeV, whereas  $\mu_n$  and  $\mu_p$  remain unaltered. The decrement in  $\mu_e$  is caused by the phase space modification of electrons in strongly quantizing magnetic field. For  $B_* = 10^4$  only the first Landau level ( $\nu = 0$ ) gets populated leading to a smaller value of  $\mu_e$  than the nonmagnetic case, for a given  $\rho_e$  [see

TABLE I. Transition densities ( $\text{fm}^{-3}$ ) at different temperatures with and without magnetic field.

$T$ (MeV)	0	1	2	3	4	5
$B_* = 0$	0.056	0.054	0.049	0.043	0.035 (0.003)	-
$B_* = 10^4$	0.055	0.053	0.049	0.044	0.039 (0.002)	0.030 (0.004)

Eqs. (25) and (26)]. Hence, the value of  $\mu_e$  required to achieve the  $\beta$  equilibrium is obtained at higher  $Y_p$ , which in turn leads to higher  $\rho_e$ . For the present example,  $Y_p$  got increased from 0.102 to 0.321 with corresponding increase in  $\rho_e$  from  $1.02 \times 10^{-4}$  to  $3.21 \times 10^{-4} \text{ fm}^{-3}$  to satisfy the  $\beta$ -equilibrium condition. Although more electrons in the system increases their kinetic energy to some extent but the nuclear energy and therefore the free energy is greatly reduced due to the reduction in the Coulomb energy. This can also be observed by noting the values of  $e_N$  and  $e_{el}$  from Figs. 1 and 2. In other words, strong magnetic field increases the binding energy of the system. This is also the reason why the solution with nuclei survives up to a higher temperature in the presence of strong magnetic fields.

In Table I, we show the maximum densities up to which nuclear cluster phase exists at different temperatures and for  $B_* = 0$  and  $10^4$ . Beyond these densities, which we call transition densities, the nuclear matter becomes fully uniform. It is found that the transition density decreases with temperature for both the magnetic and nonmagnetic cases, as expected. The transition densities at  $B_* = 10^4$  are not very different from that of nonmagnetic scenario at low temperatures ( $T = 0-3$  MeV). However, the transition density is found to be higher at  $T = 4$  for  $B_* = 10^4$ , in comparison to the field-free case. At  $T = 5$  MeV the cluster phase does not exist at all in absence of magnetic field, whereas it exists till  $0.030 \text{ fm}^{-3}$  in case of  $B_* = 10^4$ . We also note that matter becomes homogeneous at higher temperature in the lower density side as well. These lowest densities are indicated in brackets in Table I. For example, at  $T = 4$  MeV and without magnetic field the matter becomes uniform for densities below  $0.003 \text{ fm}^{-3}$ . Similarly, at  $B_* = 10^4$  the clusters do not exist below  $0.002 \text{ fm}^{-3}$  at  $T = 4$  MeV and below  $0.004 \text{ fm}^{-3}$  at  $T = 5$  MeV. This feature becomes more evident from Table II, where we have listed the transition temperature, i.e., the temperature up to which the cluster phase exists, at different density points. The transition temperature first increases with density, and decreases at higher density for both the magnetic and nonmagnetic cases. This behavior of transition temperature is consistent with the findings of other study [28]. The value of transition temperature is comparatively higher for  $B_* = 10^4$ , which can go up to 5 MeV for a density range  $0.005-0.03 \text{ fm}^{-3}$ . However, at higher densities the transition temperature are same for magnetic and nonmagnetic cases. We find that the critical

temperature defined as the highest among the transition temperatures is 4 MeV for  $B = 0$ . However, at  $B_* = 10^4$  it is 1 MeV higher.

Figure 3(a) shows the WS cell radii corresponding to free energy minima as a function of number density of nucleons for a range of temperature (0–4 MeV). The size of the cell always decreases with increasing baryon density. In fact, the WS cell size is quite large at very low density, as was also shown in Fig. 1, it shoots up at  $\langle \rho \rangle = 0.001 \text{ fm}^{-3}$  for  $T = 3$  MeV compared to zero temperature case. For  $T = 4$  MeV, however, the matter becomes completely uniform at  $\langle \rho \rangle < 0.003 \text{ fm}^{-3}$ . On the high density side ( $\langle \rho \rangle \gtrsim 0.015 \text{ fm}^{-3}$ ), at a given density the WS cell size is smaller for high temperature. Also, as expected, the nuclei dissolve into uniform matter at a relatively lower density for hot inner crust. In the presence of strongly quantizing magnetic field, the nature of the curves remains more or less similar. We see that for low densities ( $\langle \rho \rangle \lesssim 0.01 \text{ fm}^{-3}$ ) finite temperature causes the WS cell radii to increase, but the cell size is not as large as  $B = 0$  case. At a fixed temperature magnetic field reduces the cell size. This is again because at very high magnetic field the Coulomb interaction becomes much more efficient in increasing the nuclear binding energy which then plays the most dominant role in deciding the free energy minimum and thereby leading to the reduction in the cell radius than that of the field-free case. With rise in temperature more and more neutrons become unbound and drip out of the nuclei. As a result, the nuclear binding energy decreases and cell size increases.

In Fig. 3(b) we display the dependence of proton fraction on average baryon density for  $T = 0-4$  MeV and with and without quantizing magnetic field. We note that proton fraction decreases with temperature for both the nonmagnetic and magnetic cases. It is also observed that magnetic field of strength  $B_* = 10^4$  enhances the proton fraction significantly, especially at low densities. This is because strong magnetic field reduces electron chemical potential and therefore higher proton fraction is needed to maintain the  $\beta$  equilibrium. We have already discussed it in detail in connection with Figs. 1 and 2.

The top panels of Fig. 4 show the total number of nucleons  $A_{\text{cell}} (= 4/3\pi R_c^3 \langle \rho \rangle)$  inside the WS cell, as a function of baryon density in nonmagnetic (left panel) and magnetic (right panel) NS inner crust, respectively. In both the cases, the number grows to a maximum before falling down at higher

TABLE II. Transition temperature (MeV) at different density points with and without magnetic field.

density $\langle \rho \rangle$ ( $\text{fm}^{-3}$ )	0.001	0.005	0.010	0.020	0.030	0.040	0.050	0.055
$B_* = 0$	3	4	4	4	4	3	1	0
$B_* = 10^4$	3	5	5	5	5	3	1	0

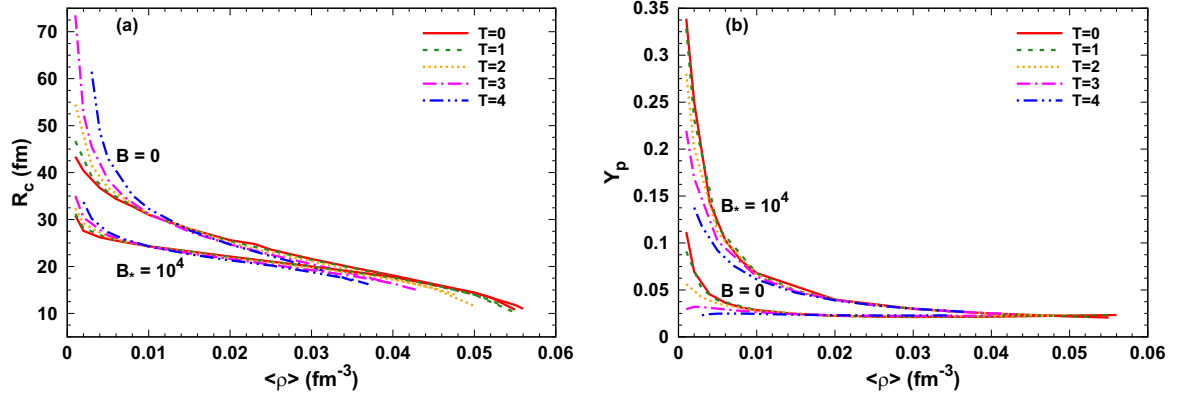


FIG. 3. (a) WS cell radius  $R_c$  and (b) proton fraction  $Y_p$  as a function of average baryon density for  $T = 0$ – $4$  MeV with and without quantizing magnetic field.

densities. These findings are consistent with earlier studies performed at  $T = 0$  [23,30,31]. In  $B_* = 0$  case, at very low density, the number shoots up for higher temperature. This is the consequence of high values of  $R_c$  at low densities, as noted earlier. At higher densities,  $A_{\text{cell}}$  is maximum at  $T = 0$  and decreases with temperature for both the nonmagnetic and magnetic cases. However, for  $B_* = 10^4$ , the cell can accommodate a lesser number of nucleons as evident from Fig. 4.

In the middle and bottom panels of Fig. 4 we plot the individual number of neutrons and protons in the WS cell, in the absence and presence of magnetic field ( $B_* = 10^4$ ). The proton number decreases monotonically with higher baryon density, whereas the total number of neutrons rises with number density, reaches a peak and falls off at higher density. Therefore, the nature of total number of nucleons curve is mostly due to number of neutrons. Both the nucleon numbers

go down for high temperature matter. At a particular density, the proton number goes up slightly for  $B_* = 10^4$  compared to nonmagnetic case. This is the consequence of higher values of proton fraction in the magnetic case as noted above. It is also seen that the number of neutrons and as a result the number of nucleons in the cell is smaller for  $B_* = 10^4$  at any given density.

We plot the total number of nucleons, protons and neutrons inside the nucleus in Fig. 5 for nonmagnetic and magnetic cases. These numbers are obtained from the subtracted densities, using Eq. (20). Number of neutrons and as a consequence  $A$  increase in the lower density part to reach a maximum, then they fall with increasing density for the entire range of temperature from  $T = 0$  to  $4$  MeV, for both the cases. The nucleus becomes smaller with temperature containing less numbers of neutrons and protons. These happen because with rise in

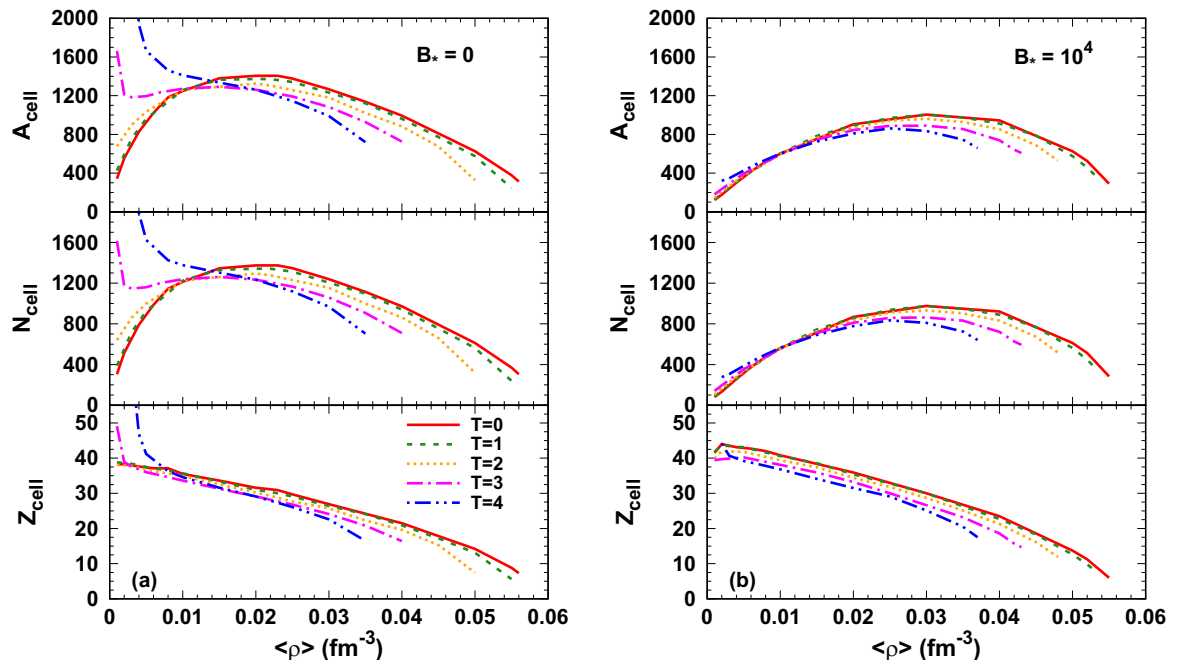


FIG. 4. Total number of neutrons ( $N_{\text{cell}}$ ), protons ( $Z_{\text{cell}}$ ) and  $A_{\text{cell}} = N_{\text{cell}} + Z_{\text{cell}}$  in the cell as a function of average baryon density and temperature for (a)  $B_* = 0$  and (b)  $B_* = 10^4$ .

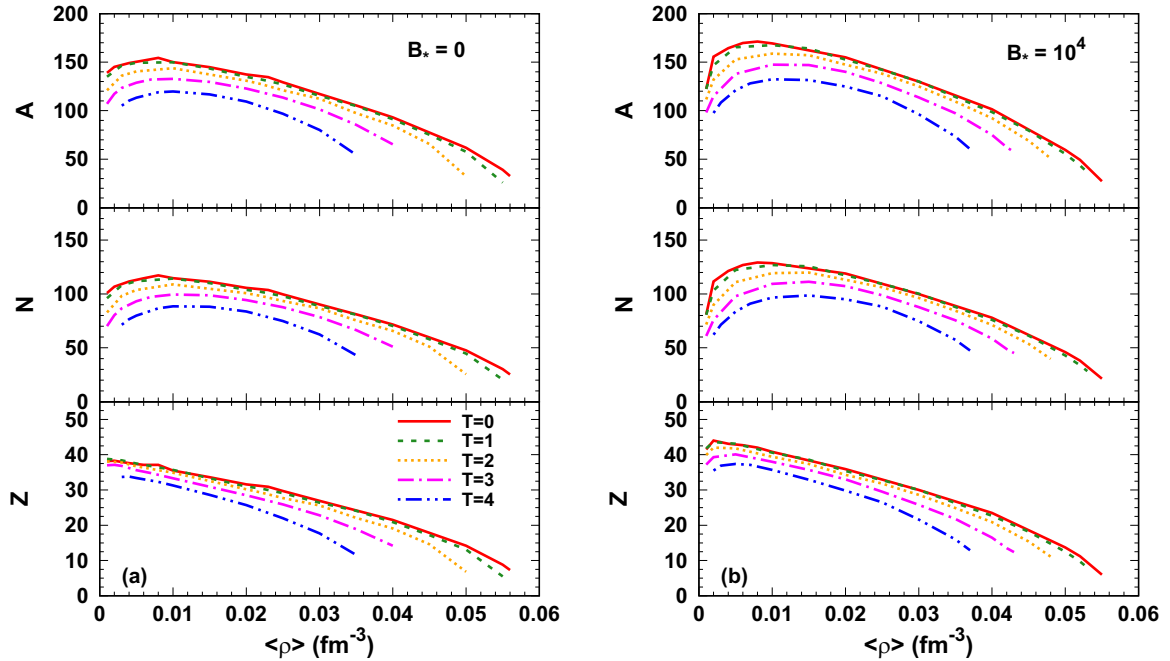


FIG. 5. Total number of neutrons ( $N$ ), protons ( $Z$ ), and  $A = N + Z$  in the nucleus as a function of average baryon density and temperature for (a)  $B_* = 0$  and (b)  $B_* = 10^4$ .

density and temperature increasing number of neutrons drip out of the nucleus. In presence of magnetic field of strength  $B_* = 10^4$  nuclei are found to be heavier having larger number of neutrons and protons at all densities and temperatures, as compared to the non-magnetic case. This is again due to the extension of neutron drip point and enhancement in proton fraction induced by the quantizing magnetic field.

Finally, in Fig. 6, we plot the minimized free energy per nucleon ( $F/A_{\text{cell}}$ ) of the system with and without magnetic field, which increases monotonically with baryon density. On the other hand, at any given baryon density  $F/A_{\text{cell}}$  is maximum at  $T = 0$ , and decreases as the temperature increases. This is mostly due to the last term in Eq. (31), which grows with temperature. For  $B_* = 10^4$  the  $F/A_{\text{cell}}$  values (see the right panel of Fig. 6) are smaller than the field free results both for  $T = 0$  and  $T > 0$  cases. The lower  $F/A_{\text{cell}}$  values

for the magnetized crust at the same density and temperature again emphasizes the greater binding energy of crustal matter in strong quantizing magnetic field [23].

#### IV. SUMMARY AND DISCUSSIONS

We have studied the effect of finite temperature and strong magnetic fields on the properties of neutron star inner crusts. We adopt the WS cell approximation where the nucleus is considered to lie at the cell center and immersed in gases of free electrons and neutrons. For the calculation of nuclear energy we use Skyrme energy density functional with SkM\* interaction. The equilibrium properties at a given density, temperature and magnetic field are obtained by minimizing the free energy per nucleon of the cell under the condition of charge neutrality and  $\beta$  equilibrium. In order to

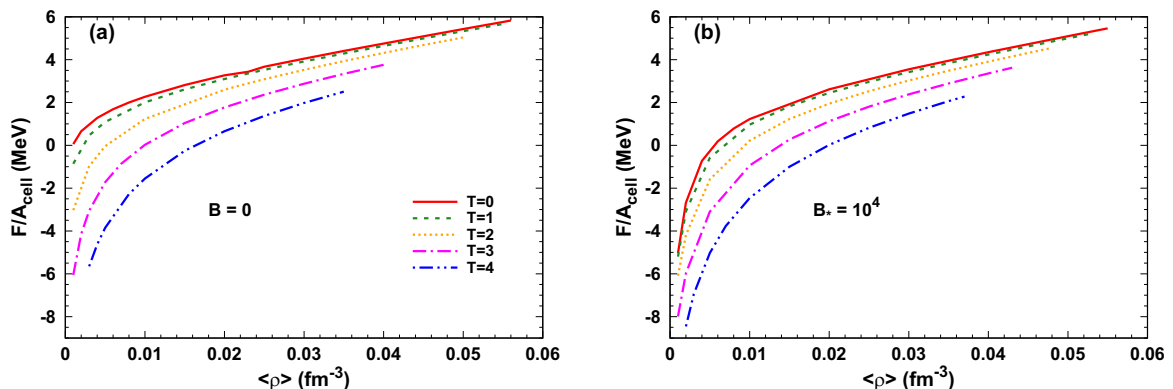


FIG. 6. Free energy per baryon as function of baryonic number density for zero and finite temperature in (a) absence and (b) presence of quantizing magnetic field.

isolate the properties of equilibrium nucleus we employ the separation procedure within TF formalism. Magnetic fields directly affects the electrons as their motion perpendicular to the direction of the field get quantized in Landau levels. The effect is significant for  $B \gtrsim 10^{17}$  G, when electrons populate only the first Landau level. This results in less number of dripped neutrons, higher proton fraction, heavier nucleus and higher binding energy in the inner crust as compared to nonmagnetic case. However, the effect of temperature is found to act in the opposite direction and reduces the impact of magnetic fields. We also find that with increasing temperature the transition to uniform matter takes place at lower density.

The dynamical ejecta of a binary neutron star merger can have two components capable of synthesizing heavy elements via  $r$  process [32]. One component is ejected because of the tidal forces and contains very neutron-rich matter emanating from cold neutron star crust. The other component is hotter as it originates due to the shock heating at the interface of two merging neutron stars. If the neutron stars possess strong magnetic fields or their initial low fields get amplified during

the merging process [24], our results can be useful to calculate the  $r$  process yields in both the scenarios. However, at finite temperature single-nucleus description may not be adequate and one needs to consider mixtures of different nuclei [33,34]. This is also manifested in our calculation as we find that the free energy does not change much with  $A$  or  $A_{\text{cell}}$  (see Fig. 1 and 2) when the temperature is high. In a future study, we plan to investigate the effect of strong magnetic fields on the composition of hot neutron star crust within a model that would allow mixture of different nuclei and Landau quantization of protons.

#### ACKNOWLEDGMENTS

S.M. and S.B. would like to acknowledge the support of DAE-BRNS Research Grant no. 37(3)/14/12/2018-BRNS. S.M. also thanks the hospitality of the Department of Physics, BITS Pilani, Hyderabad Campus where the research work was carried out.

- 
- [1] R. C. Duncan and C. Thompson, *Astrophys. J. Lett.* **392**, L9 (1992).
  - [2] V. M. Kaspi and A. M. Beloborodov, *Ann. Rev. Astron. Astrophys.* **55**, 1 (2017).
  - [3] C. Thompson and R. C. Duncan, *Mon. Not. R. Astron. Soc.* **275**, 255 (1995).
  - [4] C. Thompson and R. C. Duncan, *Astrophys. J.* **473**, 322 (1996).
  - [5] S. L. Shapiro and S. A. Teukolsky, *Black Holes, White Dwarfs and Neutron Stars* (Wiley-Interscience, New York, 1983).
  - [6] D. Lai and S. L. Shapiro, *Astrophys. J.* **383**, 745 (1991).
  - [7] A. A. Sokolov and I. M. Ternov, *Synchrotron Radiation* (Pergamon, Oxford, 1968).
  - [8] L. D. Landau and E. M. Lifshitz, *Quantum Mechanics*, 3rd. ed. (Pergamon, Oxford, 1977).
  - [9] V. Canuto and J. Ventura, *Fundam. Cosm. Phys.* **2**, 203 (1977).
  - [10] P. Mészáros, *High Energy Radiation from Magnetized Neutron Stars* (University of Chicago, Chicago, 1992).
  - [11] N. Chamel, R. L. Pavlov, L. M. Mihailov, C. J. Velchev, Z. K. Stoyanov, Y. D. Mutafchieva, M. D. Ivanovich, J. M. Pearson, and S. Goriely, *Phys. Rev. C* **86**, 055804 (2012).
  - [12] E. J. Ferrer, V. de la Incera, J. P. Keith, I. Portillo, and P. L. Springsteen, *Phys. Rev. C* **82**, 065802 (2010).
  - [13] L. Lopes and D. Menezes, *J. Cosm. Astro. Phys.* **2015**, 8 (2015).
  - [14] D. Bandyopadhyay, S. Chakrabarty, and S. Pal, *Phys. Rev. Lett.* **79**, 2176 (1997).
  - [15] J. Fang, H. Pais, S. Avancini, and C. Providência, *Phys. Rev. C* **94**, 062801(R) (2016).
  - [16] J. Fang, H. Pais, S. Pratapsi, and C. Providência, *Phys. Rev. C* **95**, 062801(R) (2017).
  - [17] J. Fang, H. Pais, S. Pratapsi, S. Avancini, J. Li, and C. Providência, *Phys. Rev. C* **95**, 045802 (2017).
  - [18] P. Bonche, S. Levit, and D. Vautherin, *Nuc. Phys. A* **427**, 278 (1984).
  - [19] P. Bonche, S. Levit, and D. Vautherin, *Nuc. Phys. A* **436**, 265 (1985).
  - [20] E. Suraud, *Nucl. Phys. A* **462**, 109 (1987).
  - [21] J. N. De, X. Vinas, S. K. Patra, and M. Centelles, *Phys. Rev. C* **64**, 057306 (2001).
  - [22] T. Sil, J. N. De, S. K. Samaddar, X. Vinas, M. Centelles, B. K. Agrawal, and S. K. Patra, *Phys. Rev. C* **66**, 045803 (2002).
  - [23] R. Nandi, D. Bandyopadhyay, I. N. Mishustin, and W. Greiner, *Astrophys. J.* **736**, 156 (2011).
  - [24] R. Ciolfi, *Gen. Rel. Grav.* **52**, 59 (2020).
  - [25] M. Brack, C. Guet, and H. B. Hakansson, *Phys. Rep.* **123**, 275 (1985).
  - [26] J. R. Stone, J. C. Miller, R. Koncewicz, P. D. Stevenson, and M. R. Strayer, *Phys. Rev. C* **68**, 034324 (2003).
  - [27] D. Lai, *Rev. Mod. Phys.* **73**, 629 (2001).
  - [28] R. Nandi and S. Schramm, *Phys. Rev. C* **95**, 065801 (2017).
  - [29] R. Nandi and D. Bandyopadhyay, *J. Phys. Conf. Ser.* **312**, 042016 (2011).
  - [30] J. W. Negele and D. Vautherin, *Nucl. Phys. A* **207**, 298 (1973).
  - [31] K. S. Cheng, C. C. Yao, and Z. G. Dai, *Phys. Rev. C* **55**, 2092 (1997).
  - [32] J. J. Cowan, C. Sneden, J. E. Lawler, A. Aprahamian, M. Wiescher, K. Langanke, G. Martínez-Pinedo and F. K. Thielemann, *Rev. Mod. Phys.* **93**, 15002 (2021).
  - [33] J. M. Lattimer, C. J. Pethick, D. G. Ravenhall, and D. Q. Lamb, *Nucl. Phys. A* **432**, 646 (1985).
  - [34] M. Hempel and J. Schaffner-Bielich, *Nucl. Phys. A* **837**, 210 (2010).